THE JOURNAL OF PHYSICAL CHEMISTRY A
A JOURNAL OF THE AMERICAN CHEMICAL SOCIETY

pubs.acs.org/JPCA

Article

Generation of Amorphous Silica Surfaces with Controlled Roughness

Nuong P. Nguyen and Brian B. Laird*

Cite This: J. Phys. Chem. A 2023, 127, 9831−9841

Read Online

ACCESS | Metrics & More | Article Recommendations | Supporting Information

ABSTRACT: Amorphous silica (a-SiO_2) surfaces, when grafted with select metals on the active sites of the functionalized surfaces, can act as useful heterogeneous catalysts. From a molecular modeling perspective, one challenge has been generating a-SiO_2 slab models with controllable surface roughness to facilitate the study of the effect of surface morphology on the material properties. Previous computational methods either generate relatively flat surfaces or periodically corrugated surfaces that do not mimic the full range of potential surface roughness of the amorphous silica material. In this work, we present a new method, inspired by the capillary fluctuation theory of interfaces, in which rough silica slabs are generated by cleaving a bulk amorphous sample using a cleaving plane with Fourier components randomly generated from a Gaussian distribution. The width of this Gaussian distribution (and thus the degree of surface roughness) can be tuned by varying the surface roughness parameter α. Using the van Beest, Kramer, and van Santen (BKS) force field, we create a large number of silica slabs using cleaving surfaces of varying roughness (α) and using two different system sizes. These surfaces are then characterized to determine their roughness (mean-squared displacement), density profile, and ring size distribution. This analysis shows a higher concentration of surface defects (under-/overcoordinated atoms and strained rings) as the surface roughness increases. To examine the effect of the roughness on surface reactivity, we re-equilibriate a subset of these slabs using the reactive force field ReaxFF and then expose the slabs to water and observe the formation of surface silanols. We observe that the rougher surfaces exhibit higher silanol concentrations as well as bimodal acidity.

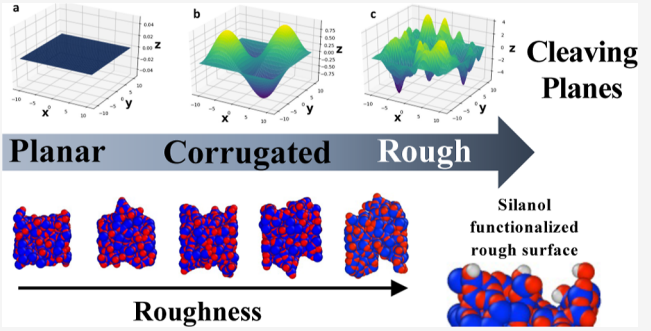

1. INTRODUCTION

Because of its high surface area, diversity of potential active sites, and high catalytic activity,[1−3] amorphous silica has proven to be an excellent support medium for metal oxide catalysts.[4] For example, Cr/SiO_2 Phillips[5] catalysts are used in the ethylene polymerization process for a significant fraction of commercial polyethylene production,[6] $Nb(V)/SiO_2$ catalysts are used in multiple chemical selective epoxidation processes,[7−10] and W/SiO_2 or Cr/SiO_2 catalysts are employed in olefin metathesis.[11]

The diverse and distinctive surface sites of amorphous silica make it difficult for the selection of active sites and rational design of silica-supported catalysts.[3,4] Over the years, there have been attempts to study the surface chemistry of silica.[12] Experimental chemists have utilized spectroscopic methods such as Raman, IR, and NMR[13−18] to study the concentration and distribution of silanol and siloxane groups or methods such as UV−vis DRS, FTIR, XPS, or ESR to study the structure and number of active sites[19,20] on the surface.

Computational tools and molecular simulation methods can provide an atomic understanding of the structure and mechanism of materials and material processes of chemical interest. Molecular dynamics (MD) simulations utilizing a variety of force fields[21−29] have been used to create and characterize bulk amorphous silica structures, as well as to generate hydroxylated surfaces through either *ad hoc* functionalization or autofunctionalization. Realistic metal-doped clusters can then be carved out of the silica slabs, a metal atom at a surface site followed by DFT geometry optimization.[30−32] Machine learning and *ab initio* calculations can help predict and select catalytic active sites for metal grafting.[33−36]

Unlike crystalline silica, amorphous surfaces can vary in surface roughness depending upon the method of preparation; therefore, the ability to create silica models with controlled roughness is necessary to fully model realistic systems. However, the current methods for the generation of model silica surfaces are not adequate for this task. For example, the

Received: July 23, 2023
Revised: September 26, 2023
Accepted: October 11, 2023
Published: November 8, 2023

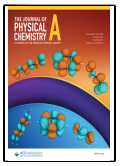

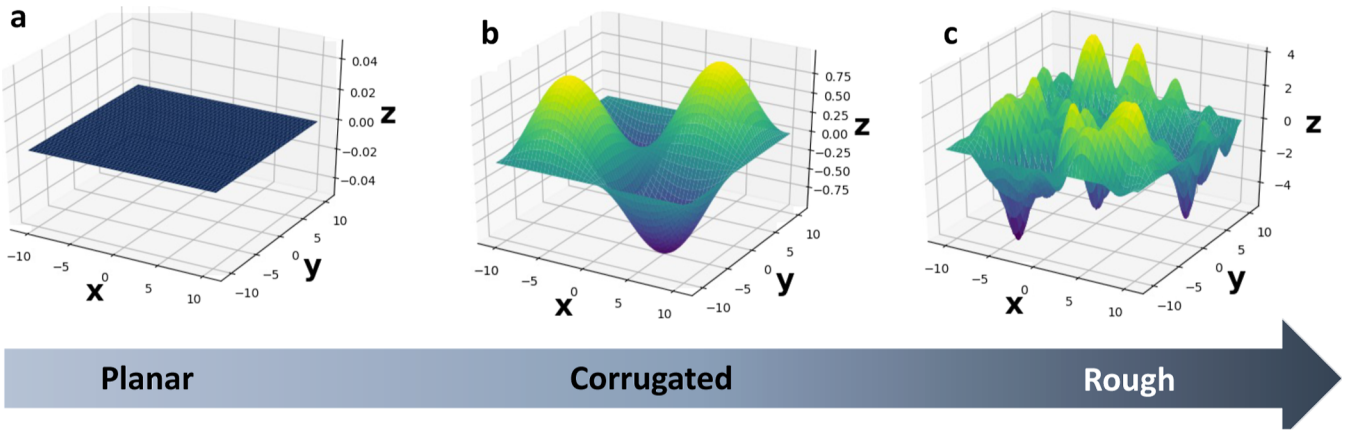

Figure 1. From left to right: planar, corrugated, and rough cleaving plane with increasing fluctuation.

most common method of generating silica slabs is the so-called *melt-quench-cleave* process in which crystalline bulk silica is melted at high temperatures (>4000 K) to obtain an amorphous structure and quenched to room temperature (298 K) where it is cleaved with a planar cleaving plane. This method, however, generates relatively flat surfaces with a limited ability to tune surface roughness. This is problematic for subsequent grafting and characterization studies because such artificially flat surfaces reduce surface area, limit the range of catalytic sites, and affect the structure and hence catalytic activity of the grafted metal clusters.[3]

Recently, Wimalasiri et al.[29] proposed a method to generate silica slabs of varying roughness using a *melt-cleave-quench* approach, in which bulk silica is first melted at a very high temperature (8000 K), followed by cleaving the system with a planar cleaving surface in the melt phase and then quenching the slabs back to 298 K at a set cooling rate. The surface roughness of the final slabs results from frozen-in capillary fluctuations of the liquid surface and is shown to be controllable through variation in the cooling rate in simulations using the BKS potential.[37] This method, while very successful at generating silica slabs of higher and more controlled roughness compared to the aforementioned "melt-quench-cleave" method, had three major drawbacks: first, besides giving varying surface roughness, the different cooling rates also gave differences in the underlying structure of the bulk region of the slabs. Second, the range over which roughness could be varied was limited, and finally, the method was not applicable to potentials for which the high temperature melt phases are unstable, such as ReaxFF.[23,38,39]

One potential solution to generate rough surfaces without having to vary the cooling rate (which affects other properties) would be to modify the melt-quench-cleave method to use a rough, not planar, cleaving surface. In an early attempt at this, Lee et al.[40] used a predefined cleaving surface consisting of a single-mode 2D sinusoidal wave, as shown below

$$z(x, y) = b \sin\left(\frac{2\pi x}{L_x}\right)\sin\left(\frac{2\pi y}{L_y}\right) \tag{1}$$

where both the amplitude b of the wave and the cross-sectional dimensions L_x and L_y, which control the peak spacing, can be adjusted. These slabs were then used to study the effect of the local surface curvature on the adsorption of polyamines to the surface. However, because only a single Fourier mode was used, the surfaces produced by this method are better described as "corrugated" as opposed to "rough".

In this work, we describe a method to generate stochastically rough cleaving planes for the production of silica slabs using the melt-quench-cleave procedure. This method takes its inspiration from the capillary fluctuation theory (CFT) description of surface fluctuations of a rough surface.[41] In CFT, the local height of the surface normal to the interfacial plane is described as a general Fourier expansion with amplitudes that are chosen from a Gaussian distribution dependent on the magnitude of the wavevector. For a normal fluctuating interface, the width of this distribution is governed by the stiffness of the interface. CFT has proven useful in the calculation of interfacial stiffness (and interfacial free energy)[42] and interface step fluctuations[43] and to determine the kinetic coefficient for near-equilibrium crystal growth.[44] Here, we use the stochastic Fourier expansion of CFT to generate rough cleaving surfaces in order to create silica slabs with controlled roughness. The difference among planar, corrugated, and rough cleaving surfaces is illustrated in Figure 1.

2. CLEAVING USING ROUGH SURFACES

2.1. Generation of Stochastic Cleaving Surfaces. Inspired by CFT,[41,42] we define a rough cleaving surface by extending eq 1 to include multiple Fourier modes

$$z(x, y) = \sum_{m=1}^{m_{max}} \sum_{n=1}^{n_{max}} b_{mn} \sin\left(\frac{m\pi x}{L_x}\right) \sin\left(\frac{n\pi y}{L_y}\right) \tag{2}$$

Here, $L_x = L_y = L$ are simulation box lengths in the x and y directions and b_{mn} is the amplitude of wave vector $\vec{k} = (k_x, k_y) = (m\pi/L_x, n\pi/L_y)$.

The maximum values m_{max} and n_{max} are chosen so that the minimum wavelength of a mode in any direction is approximately equal to the cutoff Si−O distance of 1.8 Å. As in CFT, we assume that Fourier modes corresponding to different wavenumbers are independent with amplitudes randomly distributed according to a Gaussian distribution in the magnitude of the wavevector $\vec{k} = k^2 = k_x^2 + k_y^2 = \pi^2(m^2 + n^2)/L^2$

$$P(b_{mn}) = \sqrt{\frac{\alpha(m^2 + n^2)}{2\pi}} \exp\left[-\frac{\alpha(m^2 + n^2)}{2} b_{mn}^2\right] \tag{3}$$

where we have introduced a roughness parameter α. Smaller values of α correspond to rougher cleaving surfaces. For the

https://doi.org/10.1021/acs.jpca.3c04955
J. Phys. Chem. A 2023, 127, 9831−9841

case of a dynamically fluctuating solid−liquid interface in CFT, α is inversely proportional to the surface stiffness $\tilde{\gamma}$. Here, we simply use α as a control parameter to "dial in" specific degrees of roughness. Other distributions for b_{mn} are possible, but we have chosen this one for this study because it does have a physical basis in CFT; for example, for a surface formed through the rapid quenching of a liquid slab, whose surface should fluctuate according to CFT, we would expect the surface fluctuations to be well described by a Gaussian function. Without another physical model or experimental evidence pointing to another distribution, it is difficult to speculate as to what an appropriate alternate distribution might be. The current study has as its primary purpose the introduction of the concept of the use of multimode Fourier cleaving planes to create rough surfaces and a study of multiple possible distributions is beyond the scope of this paper.

For a desired value of α, a sample cleaving surface can be generated by using eq 2 with a set of b_{mn} chosen randomly from the distribution given by eq 3. In this way, multiple independent cleaving surfaces can be created for the same value of α, allowing for the creation of silica slabs with controlled roughness. The rough silica slabs are created by inserting the cleaving surface inside the simulation box and shifting all atoms above the cleaving surface up by the z-direction box length L_z (effectively doubling the z-direction dimension to $2L_z$). The system is centered by shifting all atoms, so that the average value of z over all atoms is zero (after application of the periodic boundary conditions). For an illustration of the cleavage process, see Figure 2.

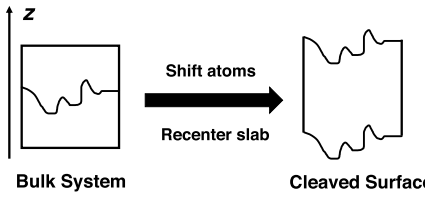

Figure 2. Illustration of silica surface generation with cleaving surfaces.

2.2. Quantification of Surface Roughness—Mean Squared Displacement. To characterize the roughness of the cleaving plane and the resulting silica slab, we utilize the mean-squared displacement (MSD) relative to the average interfacial position. The MSD of the cleaving surface itself can be determined analytically. For a given realization of the cleaving surface defined by a specific set of wave amplitudes b_{mn}, the MSD is given by

$$\overline{\delta^2 z} = \frac{1}{L_x L_y}\int_0^{L_y}\int_0^{L_x}(z(x,y)-\overline{z})^2\,dx dy = \overline{z^2}-\overline{z}^2 = \frac{1}{4}\sum_{m=1}^{m_{max}}\sum_{n=1}^{n_{max}} b_{mn}^2 - \frac{16}{\pi^4}\sum_{m=1,\text{odd}}^{m_{max}}\sum_{n=1,\text{odd}}^{n_{max}}\frac{b_{mn}^2}{m^2 n^2} \tag{4}$$

By averaging eq 4 over the entire probability distribution (eq 3), we obtain the analytical MSD associated with an ensemble of surfaces generated using a given α

$$\left\langle \overline{\delta^2 z}\right\rangle_\alpha = \int_{-\infty}^{\infty} P(b_{mn})\overline{\delta z^2}\,db_{mn} = \left\langle \overline{z^2}\right\rangle_\alpha - \left\langle \overline{z^2}\right\rangle_\alpha^2 \cong \frac{1}{\alpha}\left[\sum_{m=1}^{m_{max}}\sum_{n=1}^{n_{max}}\frac{1}{4(m^2+n^2)} - \sum_{m=1,\text{odd}}^{m_{max}}\sum_{n=1,\text{odd}}^{n_{max}}\frac{16}{\pi^4 m^2 n^2 (m^2+n^2)}\right] \tag{5}$$

The analytical multiple-configuration MSD, $\left\langle \overline{\delta^2 z}\right\rangle_\alpha$ can be used to predict the range of surface roughness of systems cleaved from a certain α value. We conducted testings at multiple α and observed that for a large enough set of cleaving surfaces, $\left\langle \overline{\delta^2 z}\right\rangle_\alpha$ is equal to the numerical MSD, calculated from data points on the cleaving surfaces with the same α.

To measure the roughness of the cleaved atomic surface, we define an atomic MSD as the average squared deviation of the z-coordinate of all surface atoms from their average height $\overline{z}$

$$\left\langle |z|^2 \right\rangle = \frac{1}{N}\sum_{i=1}^{N}(z_i(x,y)-\overline{z})^2 \tag{6}$$

where $z_i(x,y)$ is the specific height of each atom and N is the total number of surface atoms on each silica slab. The calculation of the numerical MSD is illustrated in Figure 3.

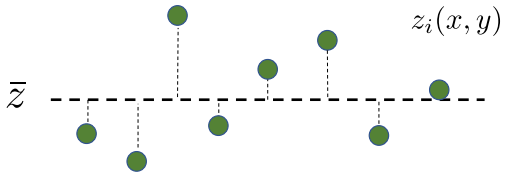

Figure 3. Illustration of the calculation of the numerical MSD, with green circles being the surface atoms and vertical dashed lines representing the perpendicular distance between the z-positions of those surface atoms to their average height, as shown by the horizontal dashed line.

A probing method is used to detect silica surface atoms. The x−y cross-sectional plane is divided into square grids with a side width of 0.3 Å. At each grid, from the vacuum space above or below the slab, a spherical probe with contact radii of 1.04 Å for Si and 0.76 Å for O approaches the surface with a distance increment of 0.05 Å. The first atom to make contact with the probe in each grid is designated to be a surface atom.

3. SIMULATION METHODS

3.1. Force Fields. In this work, we utilize two different silica potentials. The first is the BKS potential due to van Beest, Kramer, and van Santen.[37] The BKS force field is a pairwise potential commonly used in modeling crystalline and amorphous silica and is generated by combining *ab initio* calculations on small silica clusters, which allows for nearest neighbor interactions with experimental data on larger systems to account for interactions beyond nearest neighbors. The potential has the following form

$$V(r_{ij}) = A_{ij}e^{-b_{ij}r_{ij}} - \frac{c_{ij}}{r_{ij}^6} + \frac{q_i q_j}{r_{ij}} \tag{7}$$

https://doi.org/10.1021/acs.jpca.3c04955
J. Phys. Chem. A 2023, 127, 9831−9841

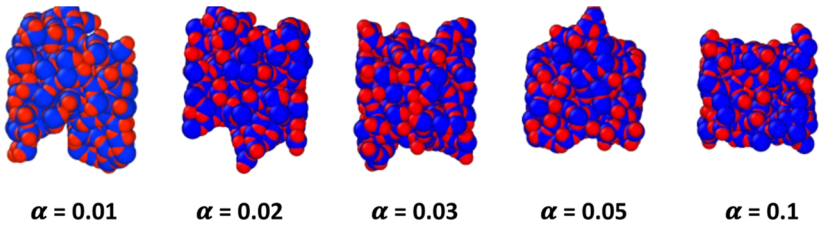

Figure 4. Rough surfaces, cleaved with different roughness parameters (α = 0.01, 0.02, 0.03, 0.05, and 0.1 Å^{-2}, from left to right) and re-equilibrated with the BKS force field.

Equation 7 describes the pair interaction between atom i and j of interatomic distance r_{ij}. The first two terms describe the short-range interaction in the Buckingham form, while the third term represents long-range Coulombic interactions. Atomic charges are defined such that $q_O = -q_{Si}/2$ to maintain charge neutrality of the system. Specific parameters used in this paper such as q_{Si}, q_O, A_{ij}, b_{ij}, c_{ij}, Coulombic term electrostatic cutoff, and other parameters were taken from our previous paper.[29]

The second potential used in this work is ReaxFF,[23,38,39] which is a bond-order-based reactive force field developed by van Duin et al.[23] to describe chemical reactions, as well as to model systems more realistically due to the ability to model bond formation and dissociation and to update atomic charges at every step.

The system energy described by ReaxFF is the sum of multiple energy terms

$$E_{system} = E_{bond} + E_{over} + E_{under} + E_{lp} + E_{val} + E_{tors} + E_{vdW} + E_{Coul} \quad (8)$$

Apart from the nonbonding terms that exist in classical force fields such as van der Waals term (E_{vdW}) and Coulombic term (E_{Coul}), ReaxFF also introduces bonding energy terms that account for bonding (E_{bond}), over- and under-coordination (E_{over} & E_{under}), lone pair (E_{lp}), valence angle (E_{val}), and torsion (E_{tors}). These bonding energy terms are calculated based on the bond order, which is directly calculated from interatomic distances of atoms. The bond order is updated continuously, allowing for bond formation and breaking.

Because of its properties, the ReaxFF force field effectively bridges the gap between computationally expensive quantum calculation methods and less accurate nonreactive classical force fields. Multiple MD simulations have used the ReaxFF force field to study the interaction of silica and water.[26,27,45−47] In this paper, ReaxFF was used to model the autofunctionalization process of amorphous silica surfaces when exposed to water. Force field parameters were taken from the 2010 Fogarty et al. paper,[24] where trained Si/O/H bond parameters and angle parameters from the 2003 ReaxFFSiO paper[39] were refitted to include proton−transfer reactions at the silica/water interface.

3.2. Simulation Details. All MD simulations in this paper were carried out using the Large scale Atomic/Molecular Massively Parallel Simulator (LAMMPS) software package.[48]

The simulations begin with an initial bulk amorphous silica sample, consisting of 576 atoms (192 Si and 384 O atoms), which was generated by heating a β-cristobalite structure at constant pressure (1 atm) to 8000 K using the BKS force field, followed by cooling to 298 K at a rate of 1 K/ps.[29] This bulk silica sample was then melted and equilibrated at 4000 K for 200 ps using an NP_zAT ensemble and then cooled to 298 K with a cooling rate of 1 K/ps using 10 different random velocity seeds to generate 10 different bulk amorphous silica structures. For these simulations, the cross-sectional dimensions are held fixed to simplify the analysis, with $L_x = L_y$ = 21.0 Å. In addition, a Berendsen thermostat (damping constant 1 ps) and a Berendsen barostat (damping constant 1 ps, modulus 360,000 atm) were employed.

Using the cleaving algorithm described in Section 2, each of these 10 bulk samples was cleaved with 10 randomly generated cleaving surfaces placed at 10 different height positions, with chosen α values of 0.01, 0.02, 0.03, 0.05, and 0.1 Å^{-2}, resulting in 100 silica slabs for each α. The cleaved silica slabs were then equilibrated for 2 ns by using the NP_zAT ensemble. Figure 4 illustrates equilibrated silica slabs cleaved with cleavage planes of different α values.

We also generated an additional set of 100 silica surfaces using the standard melt-quench method and a planar cleaving surface ($\alpha = \infty$).[24] In this set, surfaces were created by cooling the previously generated bulk liquid silica sample using the NP_zAT ensemble with a cooling rate of 1 K/ps and expanding the simulation box in the z direction to 80 Å, allowing for planar surface cleaving. The surfaces were then re-equilibrated at 298 K for 200 ps, also using the $NPzAT$ ensemble. Coordinates for all generated slabs can be found in the Supporting Information.

To examine the effect of system size, we generated a larger bulk silica sample by doubling the length of the simulation box in the x and y directions (42.0 × 42.0 Å^2), yielding a system with four times the number of atoms (2304 atoms). With this bulk sample, we applied the same cleaving protocol as described above to rough and planar surfaces. The set of cleaving roughness parameters (α) for this larger system have values of 0.008, 0.01, 0.02, 0.03, 0.05, 0.1 Å^{-2}, and ∞ (planar). In the next section, the atomic MSDs of surfaces generated with planar and fluctuating cleaving surfaces will be compared with those of the smaller size—because the larger size allows for smaller wavevectors, it is expected that the MSD of the larger systems will increase roughly logarithmically with the surface area.[49] (This can be seen by approximating the sums in eq 5 by integrals and integrating using polar coordinates.)

In order to study the effect of roughness on surface reactivity, we re-equilibrated our slabs using the ReaxFF reactive potential. The ReaxFF force field allows for the breaking and formation of bonds. (For more information on the ReaxFF force field, see Section 3.1.) Here we expose the re-equilibrated slabs to water, which will react with under/over-coordinated atoms at the surface to form surface silanol groups. In the silica−water reactive simulations, a bulk sample of 200 water molecules was generated with the initial density of 1.0 g/cm^3 using Packmol software[50] in a simulation box with cross-sectional dimensions identical to that of the silica slabs. The bulk water sample was equilibrated using the ReaxFF force

https://doi.org/10.1021/acs.jpca.3c04955
J. Phys. Chem. A 2023, 127, 9831−9841

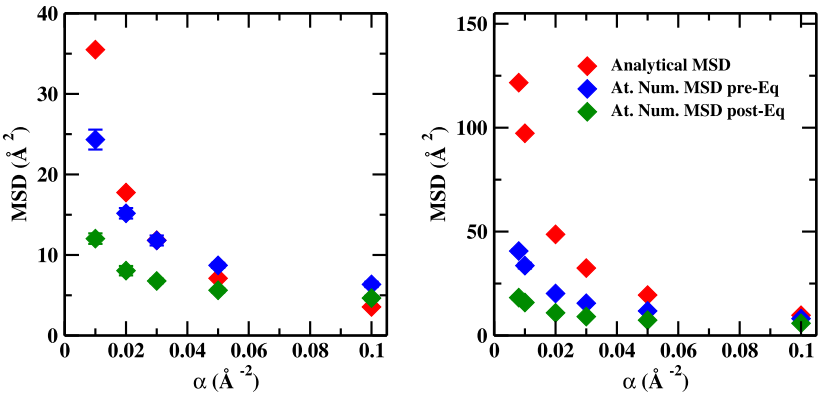

Figure 5. MSD surface roughness of amorphous silica surfaces immediately after cleavage (black) and after re-equilibration (red). Left panel: smaller system and right panel: larger system.

field with the NP_zAT ensemble at 298 K for 200 ps. Also using the Packmol software, 10 equilibrated rough surfaces from the set cleaved with α = 0.02 and 0.1 Å^{-2} and planar surfaces were then placed adjacent (in the z direction) to the equilibrated bulk water sample with an initial interfacial distance of 2.5 Å in the z-direction. These silica−water simulations were run within the NP_zAT ensemble at 298 K and 1 atm using the ReaxFF force field for 1.5 ns with a time step of 0.5 fs.

4. RESULTS AND DISCUSSION

In this section, we present results that show that we are able to successfully produce surfaces with controlled roughness. In addition, we examine the effect of surface roughness on silica surface structures and the reactivity of the rough surfaces with water. Section 4.1 presents atomic and numerical MSD data for both the small and large systems to examine the surface MSD as a function of roughness parameter α and to assess the effect of system size. This is followed by an in-depth atomic-level analysis of the silica surfaces of the smaller system in Section 4.2, including a characterization of the bond-distance and angle distributions, density profiles, and surface defects, specifically under/over-coordinated atoms and strained rings. In Section 4.3, we examine the reactivity of these rough surfaces when exposed to water using the ReaxFF force field in order to understand the effect of surface roughness on silanol formation on the exposed surface.

4.1. Surface Roughness. Figure 5 shows the MSD versus α for the small and large systems, respectively. Here, we compare three values of interest, the analytical MSD (red), the numerical MSD of actual silica surfaces before (blue) and after (green) re-equilibration. MSDs for the planar cleaved surfaces are 4.01(19) Å^2 (before re-equilibration) and 3.7(2) Å^2 (after re-equilibration) for the smaller system and 4.4(2) Å^2 (before re-equilibration) and 4.0(2) Å^2 (after re-equilibration) for the larger system. Here and in what follows, the numbers in parentheses represent the error estimates (2σ) in the last digits shown.

For both figures, all three data sets follow the same trend: smaller α corresponds to higher MSD values, indicating rougher surfaces. This agrees with our theoretical MSD calculation shown in eq 5. The atomic MSD values for the actual silica surfaces are lower than the theoretical ones because unlike the cleaving surfaces, silica surfaces are not continuous but have a discrete atomic structure. Silica surfaces are defined by a Si−O bond network with the average bond distance of 1.62 Å.[51] Some fluctuations take place in the gaps between atoms, making no impact on surface cleaving and therefore are not captured by atomic MSDs. Note that the MSD values for the larger system are considerably larger than those for the smaller system, as expected.

As we approach higher α values (toward ∞), the cleaving surface approaches a flat plane and the analytical MSDs decrease and eventually approach 0, while atomic MSDs plateau at 1.5 Å as a result of the intrinsic discrete atomic structure of the amorphous silica surface. If this cleaving method is applied on systems where atoms are more densely packed, we can expect to see a smaller gap between atomic MSD and analytical MSD. The atomic MSD of surfaces after re-equilibration is lower than that of those before re-equilibration because the process rearranges silica surfaces and partially resolves dangling bonds formed as a result of surface cleaving.

Henke et al.[52] used atomic force microscopy and observed a root-mean-squared displacement (rmsd) roughness for fused silica glass samples with a surface area of 5 × 5 μm^2 to be in the range of 0.2−1 nm. It is slightly difficult to compare rmsd values for systems of different sizes, but for a Gaussian distribution, we would expect the rmsd to roughly scale with the logarithm of the system size; therefore, it is possible to estimate what the expected roughness would be if we could extend our method to systems on the order of the experiments. In this paper, we chose our roughness parameters α to be in the 0.08−0.1 Å^{-2} for our silica system. Using the same range of α to cleave 5 × 5 μm^2 silica slabs, we can generate silica surfaces with an estimated rmsd in the 0.61−2.23 nm range, which is within the range of the experiment. More importantly, we can tune α to generate surfaces as rough or flat as desired.

In the next subsection, we examine how surface roughness affects the properties of the amorphous surface.

4.2. Surface Characterization. The current method to use stochastic, rough cleaving surfaces allows for a systematic study of the effect of roughness on surface properties that is possible only to a limited extent using planar or corrugated cleaving surfaces.

Mass- and coordination-density profiles along the z-direction of the equilibrated surfaces are shown in Figure 6, to provide structural insights into surfaces with varying roughness parameters. These density profiles were calculated by binning and averaging the atomic mass and the calculated atomic coordination number of Si and O atoms along the z-direction with a bin width of 1 Å. In both figures, plots of silica slabs with smaller α have more spread-out tails, a consequence

https://doi.org/10.1021/acs.jpca.3c04955
J. Phys. Chem. A 2023, 127, 9831−9841

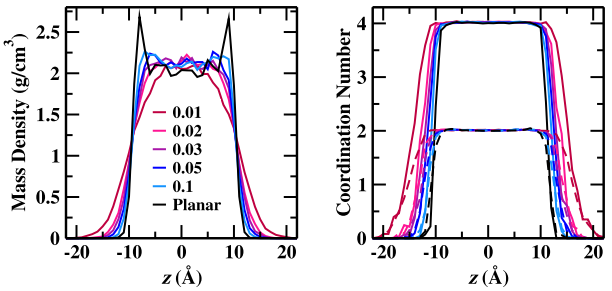

Figure 6. Mass density and coordination density profile along the z direction of silica slabs.

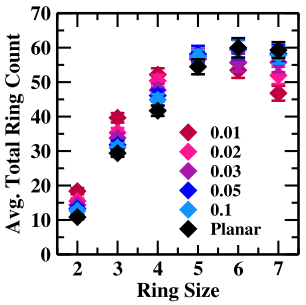

Figure 8. Average total ring count, with the number of Si atoms ranging from two to seven per ring. The number of members indicates the number of Si atoms. Rougher surfaces have higher numbers of two- and three-membered rings. They are strained rings that occur on the surface, contributing to surface roughness and strained bond angles, as shown in Figure 7.

of larger surface fluctuations for rougher surfaces. In the mass-density profile graph, the regions where mass density has small fluctuations right below the 2.25 g/cm^3 mark are the bulk silica regions. The bulk density of amorphous silica generated with the BKS force field agrees well with the mass density of 2.20 g/cm^3 for experimental data.[51] For rougher surfaces, the bulk silica regions are narrower, indicating wider surface widths. These surface widths in those plots are consistent with the MSD values in Figure 5. The two sharp peaks on the ends of the mass density profile of silica slabs with planar cleaving surfaces reflect the intrinsic shape[53] of the silica surface, which is washed out in the rougher surfaces in the averaging process.

Atoms in the bulk central region (-10 Å $< z <$ $+10$ Å) have ideal coordination numbers of 4 and 2, for Si and O, respectively. Rougher surfaces also have more over- and under-coordinated surface Si atoms (coordination numbers 3 and 5) as well as O atoms (coordination numbers 1 and 3). These over- and under-coordinated atoms are surface atoms resulting from the breaking of bonds in the cleaving process, as discussed later in this section.

The generated silica slabs can also be characterized by bond-distance and bond-angle distributions. Full distributions of Si−O bond distances, Si−O−Si bond angles, and O−Si−O bond angles are shown in Figure 7 The distribution of the Si−O−Si angle is bimodal, with a primary peak centered around 145° and a secondary peak centered around 95°. For rougher silica surfaces, we observed a minor shift of the primary peak position toward small angles and a shift of probability density into the secondary peak.

We also examine the number of ..Si−O−Si−O.. rings present in each slab as a function of surface roughness. The size of each ring is defined as the number of Si atoms in the ring. In Figure 8, we plot the total number of rings in each slab, averaged over all slabs of a given roughness. Du and Cormack[54] showed that an increase in the Si−O−Si angle distribution in the secondary peak corresponds to a higher fraction of two-membered rings, while the shift in the primary peak correlates with an increase in the fraction of three- and four-membered rings, which have average Si−O−Si bond angles of 130.5 and 146°, respectively.[55] The plot of the average total ring count in our system (Figure 8) shows that rougher silica surfaces have higher numbers of strained, smaller (two- and three- membered) rings, and four-membered rings, while having fewer larger (five-, six-, and seven-membered) rings. Previous studies showed that strained rings, along with coordination defects, tend to appear near the surface of the slabs.[22,56,57]

Table 1 summarizes the percentages of various atomic defects within the silica slabs, including fractions of over-/under-coordinated atoms and the average strained ring count. Overall, there is a decrease in all defect parameters as surface roughness decreases. Comparing the sets of roughest and flattest (planar) surfaces, we only see a minor increase in the number of under-coordinated atoms: fewer than 1 atom for three-coordinated Si and about 2 atoms for NBO. We see a slightly higher increase in the number of overcoordinated, with about 3 and 6 atoms for five-coordinated Si and three-coordinated O, respectively. The defect types that show the largest change are two-membered rings, with an increase of 15 Si atoms involved, and three-membered rings, with an increase of up to 33 Si atoms involved. This can be explained by the fact that surfaces that are roughly cleaved would have higher surface areas and therefore more dangling surface atoms. During re-equilibration, the surfaces rearrange and dangling atoms that are near to each other may recombine to form strained rings.[54,58] This surface rearrangement also explains the decrease in the MSD of the silica surfaces after re-equilibration seen in Figure 5. Three-coordinated Si, NBO, and two-membered rings are crucial for determining hydroxylation performance of silica surfaces when exposed to water, and they

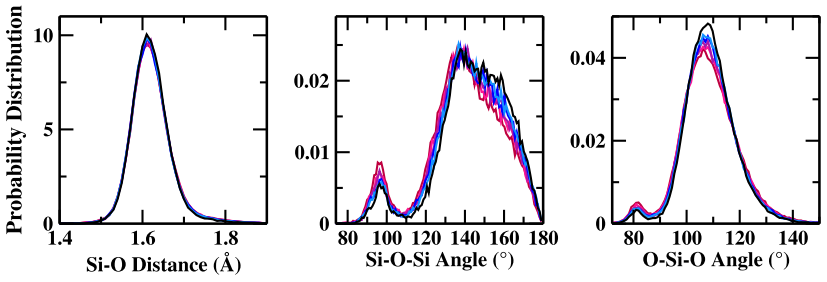

Figure 7. From left to right: Si−O bond distance (Å), Si−O−Si bond angle (deg), and O−Si−O bond angle (deg) distributions of silica surfaces.

https://doi.org/10.1021/acs.jpca.3c04955
J. Phys. Chem. A 2023, 127, 9831−9841

Table 1. Percentage of Various Defect Types in the Generated Slabs[a]

	under/over-coordinated atoms				strained rings	
α (Å^{-2})	% ^{3}Si	% ^{5}Si	% ^{1}O	%^{3}O	2-MR	3-MR
0.01	1.8(2)	2.8(3)	2.42(13)	3.0(2)	18.4(9)	39.7(1.4)
0.02	1.6(2)	2.8(3)	2.2(2)	2.8(2)	15.5(8)	35.4(1.3)
0.03	1.6(2)	2.2(3)	2.14(10)	2.5(2)	14.3(7)	33.8(1.3)
0.05	1.6(2)	2.2(3)	2.0(2)	2.4(2)	13.3(8)	31.8(1.2)
0.1	1.4(2)	1.9(3)	1.9(2)	2.2(2)	12.7(8)	31.0(1.2)
planar	1.6(2)	1.0(2)	1.8(2)	1.5(2)	10.8(6)	29.4(1.0)

[a]Included are percentages of three-coordinated Si (^{3}Si), five-coordinated Si (^{5}Si), NBO (^{1}O), three-coordinated (^{3}O), and the average total count of two-membered rings (2-MR) and three-membered rings (3-MR). The numbers in parentheses denote the error estimates (95% confidence) in the last digits shown.

will be discussed in more detail in Section 4.3. Three-coordinated O atoms were found to be associated with three-membered rings.[56] Levine and Garofalini in their MD simulation study[22] found that five-coordinated Si atoms are often found in regions with significant surface reconstruction. Other computational studies also suggested that five-coordinated Si atoms participate in three-membered rings.[59,60] Si−O bonds that are involved with these ^{5}Si form a trigonal bipyramidal geometry[61,62] that can be stabilized when grafted with zinc oxide species.[63] Three-membered rings contribute greatly to the increase in silica surface roughness as they are planar rings,[64] and instead of laying flat on the surfaces, they stand axially and hence contribute to surface fluctuations. Indeed, Brinker et al.[65] have commented that, based on a spectroscopy study by DeMayo et al.,[66] three-membered ring sites are responsible for surface inhomogeneities.

4.3. Functionalization of Silica Surfaces through Reaction with Water. After the silica surfaces are exposed to water using the ReaxFF force field, we observe the silanol concentration as a function of the time and surface roughness. Figure 9 shows the growth in silanol concentration with time for hydroxolated surfaces cleaved with α = 0.02 Å^{-2}, α = 0.1 Å^{-2} and planar cleaving planes. These values are averaged over ten sample surfaces for each value of α. In the figure, we distinguish between three classes of silanols: geminal silanols with two hydroxyl groups on the same Si atom, vicinal silanols in which two single silanols are formed on two adjacent Si atoms, and isolated silanols. In addition, the total silanol concentration (the sum of the concentration of all three classes) is also shown.

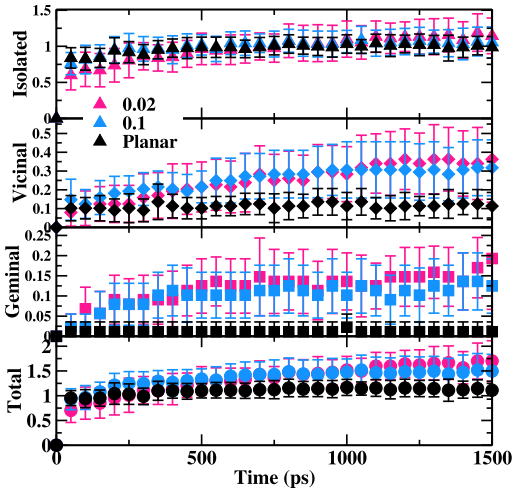

Figure 9. Time-dependent silanols growth for silica with α = 0.02 Å^{-2} (pink) and 0.1 Å^{-2} (blue) and planar cleaving (black).

After 1.5 ns, surfaces cleaved with α = 0.02 Å^{-2} have the largest number of silanols formed, followed by those cleaved with α = 0.1 Å^{-2} and then planar surfaces. This order can be explained by the fact that the rougher surfaces have higher defect fractions (as shown in Table 1). These defects are more reactive when exposed to water, compared to the hydrophobic siloxanes' planar silica surfaces. Moreover, during hydroxylation, surfaces relax and surface energies decrease, as shown in various computational studies.[46,67−70]

The total, geminal, vicinal, and isolated silanol concentrations for all three sets are consistent with a previous ReaxFF study, where 40% of surface defects were hydroxylated.[46] Rimsza et al.[26] estimated that it would take up to tens of nanoseconds to fully hydroxylate silica surfaces with ReaxFF simulations. When fully hydroxylated, the total silanol concentration is expected to reach 4.6/nm^2 as reported in an experimental study by Zhuravlev.[12,71] An MD simulation study with ReaxFF by Yeon and van Duin[27] suggested that the rate of silanol formation can be accelerated by increasing the simulation temperature to 900−1100 K for optimal silanol formation. When exposed to water, NBOs, three-coordinated Si, and strained two-membered rings were observed to quickly disappear through silanol formation.[72] Geminal silanols are formed on three-coordinated Si atoms that are also bonded to an NBO. A water molecule can attach its O atom onto an under-coordinated Si atom and donate one of its H atoms to a nearby nonbridging or siloxane O atom, as illustrated in eqs 9 and 10. The water molecule can also donate its H to another water molecule that can subsequently donate an H atom to form another silanol through hydronium dissociation[27]

$$\mathrm{Si{+}H_2O \rightarrow Si-OH + H^+} \quad (9)$$

$$\mathrm{Si-O^- + H^+ \rightarrow Si-OH} \quad (10)$$

Yeon and van Duin[27] found that hydroxyl formation favors high-strain sites, for example, two- and three-membered rings, with the hydroxylation reaction barrier of strained sites to be 10 kcal/mol lower than that of nonstrained sites. Hydroxylation of two-membered rings results in siloxane bond breakage and formation of vicinal silanols.[45] These vicinal silanols can be condensed to form siloxane during high temperature treatments,[12,73] as shown in eq 11. Compared to nonstrained siloxane sites, three-membered rings, while considered strained rings, are only 10 times more reactive to water, while two-membered rings are 10^5 times more reactive.[74] In fact, D'Souza and Pantano found that the

https://doi.org/10.1021/acs.jpca.3c04955
J. Phys. Chem. A 2023, 127, 9831−9841

hydrolysis of three-membered rings acts as the rate-determining step for full silica hydroxylation.[75] The silanol concentration of partially hydroxylated silica surfaces before three-membered ring hydrolysis was determined experimentally to be 2.6 nm^{-2}.[58,76]

$$Si - OH + H_2O \rightarrow Si - O^- + H_3O^+ \quad (11)$$

Also observed in the simulation is the temporary acid ionization of the silanol groups. This usually occurs for convex geminal silanols or out-of-plane vicinal silanols with very low pK_a values.[77,78] Those silanol O atoms, after losing its H, quickly receive another H from water through proton hopping.[27] This phenomenon explains the minor fluctuations in the silanol concentrations in Figure 9.

Figure 10 is a snapshot of a silica slab with a cleaving parameter of $\alpha = 0.02$ Å $^{-2}$, before and after hydroxylation. We

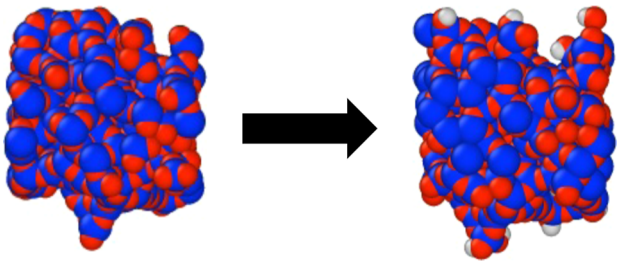

Figure 10. Sample silica slab ($\alpha = 0.02$ $Å^{-2}$) before and after surface functionalization.

can see that the slab still maintains its surface roughness. This is because only two-membered rings are broken, while three-membered rings are not. Planar three-membered rings occur on the surface of the slabs and are responsible for many of the surface fluctuations. The fact that rough silica surfaces do not change their shapes even after undergoing MD simulations with ReaxFF, a reactive potential known for its ability to break and form bonds shows that surfaces cleaved by our cleaving methods are very stable after re-equilibration with BKS. Both in-plane (high pK_a) and out-of-plane (low pK_a) silanols are observed, indicating bimodal acidicity behavior.[77−79] Figure 11 shows the distribution of the Si−O−H angles for three sets of data. Observed are a predominant peak centered at 118° and a smaller peak at 90° representing out-of-plane and in-plane silanols, respectively, confirming the bimodality in the acidicity

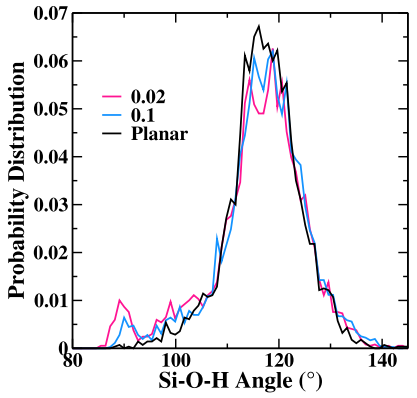

Figure 11. Silanol Si−O−H angle distributions. Those of roughly cleaved surfaces (pink and blue) show bimodal acidicity with out-of-plane and in-plane silanols.

of silanols. We do not observe in-plane silanols in the planar cleaved surfaces. A possibility could be the lack of geminal silanols, if we assume that not all geminal silanols take convex shape in our simulations, but this possibility is quite low and more extensive investigations need to be done before a definitive conclusion can be made.

Similar to our data in Figure 11, the silanol angle distribution presented in an MD study by Du and Cormack[54] on planar silica surfaces is unimodal with one dominant peak centered at 122°, indicating no in-plane silanols. This suggests that the increase in surface roughness may have improved the structural and chemical diversity of the silica surfaces. Gierada et al. carried out an *ab initio* study on amorphous hydroxylated silica surfaces and concluded that due to the complexity of the system, the acidicity of silica surfaces can not be simply determined with any single silanol type (geminal, vicinal, and isolated) but rather requires a deeper understanding of the geometries of those silanols and the H-bond network they are involved in.[80] Previously, Jystad et al.[31,32] carried out DFT studies to characterize the surface acidity of metal-doped amorphous silica catalysts. In the future, more in-depth studies on the acidity of rough hydroxylated amorphous silica surfaces will be useful in the prediction of active sites for metal grafting in the generation of silica-based catalysts.

5. CONCLUSIONS

In this paper, we present a method, inspired by the CFT of surfaces,[41] to generate model amorphous silica surface slabs of controlled roughness. The slabs are generated by cleaving bulk silica slabs using rough cleaving surfaces with Fourier components (eq 2) generated randomly from a Gaussian distribution in the wavevector magnitude whose width is controlled by a "roughness parameter" α; see eq 3. (The smaller the value of α, the rougher the cleaving surface ($\alpha = \infty$ corresponds to a planar cleaving surface). By varying α, we can control the roughness of the resulting silica surface. This method is a generalization of previous methods that used either a planar cleaving surface or a single Fourier mode "corrugated" surface. For each roughness parameter value α, ranging between 0.08 and 0.1 $Å^{-2}$, multiple different cleaving surfaces were generated that were then used to cleave bulk silica samples. The mean squared displacement and structural properties of silica surfaces cleaved with this method were compared with those of silica surfaces cleaved with a planar cleaving plane, a common method used in previous computational studies of amorphous silica. Calculations of the theoretical analytical mean squared displacements and surface atomic numerical mean squared displacements validate our method and show that we can generate silica surfaces of controlled roughness through the variation of the single parameter α, allowing for the systematic study of the effect of surface roughness on surface properties such as defect concentrations and reactivity.

Structural characterization, including calculations of density profiles, bond distance and angle distributions, ring counts, and atom coordination number, shows a higher concentration of structural defects, such as under- and over-coordinated atoms and strained two- and three-membered rings for rougher surfaces. These structural defects exist almost exclusively at or near the surface, as rougher cleaving planes with a higher surface area cleaving bulk silica result in more dangling bonds. Atoms with these dangling bonds either stay under-

https://doi.org/10.1021/acs.jpca.3c04955
J. Phys. Chem. A 2023, 127, 9831−9841

coordinated or recombine with neighboring atoms to form two- or three-membered rings with strained siloxane bonds.

When silica slabs generated with α = 0.02, 0.1 Å^{-2}, and ∞ (planar) cleaving surfaces are exposed to water using a ReaxFF reactive force field, it is observed that rougher surfaces react more quickly and exhibit increased silanol formation upon reaction with water. This is because rougher surfaces have higher concentrations of defect sites, which react more readily with water to form surface silanol groups than flatter interfaces. Distributions of silanol angles show bimodal acidicity for rough surfaces, as opposed to silanols on the planar silica surfaces with a single acidicity mode. Further studies are warranted on the effect of surface roughness on silica surface chemistry to aid in the rational design of silicate-based heterogeneous catalysts.

■ ASSOCIATED CONTENT

Supporting Information

The Supporting Information is available free of charge at https://pubs.acs.org/doi/10.1021/acs.jpca.3c04955.

Coordinates for the silica surfaces generated in this work (ZIP)

■ AUTHOR INFORMATION

Corresponding Author

Brian B. Laird − *Department of Chemistry and Center for Environmentally Beneficial Catalysis, University of Kansas, Lawrence, Kansas 66045, United States;* orcid.org/0000-0003-1859-732X; Email: blaird@ku.edu

Author

Nuong P. Nguyen − *Department of Chemistry and Center for Environmentally Beneficial Catalysis, University of Kansas, Lawrence, Kansas 66045, United States*

Complete contact information is available at: https://pubs.acs.org/10.1021/acs.jpca.3c04955

Notes

The authors declare no competing financial interest.

■ ACKNOWLEDGMENTS

The authors thank Dr. Pubudu Wilmalasiri and Profs. Ward Thompson, Marco Caricato, and Baron Peters for many useful discussions. This work was funded by the Division of Chemical Sciences, Geosciences, and Biosciences, Office of Basic Energy Sciences of the U.S. Department of Energy through grant no. DE-SC0019488. The calculations were performed at the University of Kansas Center for Research Computing (CRC), including the BigJay Cluster resource funded through NSF grant MRI-2117449.

■ REFERENCES

(1) Parmaliana, A.; Frusteri, F.; Miceli, D.; Mezzapica, A.; Scurrell, M.; Giordano, N. Factors Controlling the Reactivity of the Silica Surface in Methane Partial Oxidation. *Appl. Catal.* **1991**, *78*, L7−L12.

(2) Matsumura, Y.; Moffat, J. B.; Hashimoto, K. Activation of Surface Lattice Oxygen in the Oxidation of Carbon Monoxide on Silica. *Faraday Trans* **1994**, *90*, 1177.

(3) Groppo, E.; Lamberti, C.; Bordiga, S.; Spoto, G.; Zecchina, A. The Structure of Active Centers and the Ethylene Polymerization Mechanism on the Cr/SiO_2 Catalyst: A Frontier for the Characterization Methods. *A Frontier for the Characterization Methods* **2005**, *105*, 115−184.

(4) Goldsmith, B. R.; Peters, B.; Johnson, J. K.; Gates, B. C.; Scott, S. L. Beyond Ordered Materials: Understanding Catalytic Sites on Amorphous Solids. *ACS Catal.* **2017**, *7*, 7543−7557.

(5) Hogan, J. P.; Banks, R. L. *Polymers and Products Thereof*, 1958;.

(6) The Freedonia Group. *World Polyethylene, Industry Study with Forecast for 2018 & 2023*, 2014;.

(7) Tiozzo, C.; Palumbo, C.; Psaro, R.; Bisio, C.; Carniato, F.; Gervasini, A.; Carniti, P.; Guidotti, M. The Stability of Niobium-Silica Catalysts in Repeated Liquid-Phase Epoxidation Tests: A Comparative Evaluation of in-Framework and Grafted Mixed Oxides. *Inorg. Chim. Acta* **2015**, *431*, 190−196.

(8) Somma, F.; Canton, P.; Strukul, G. Effect of the Matrix in Niobium-Based Aerogel Catalysts for the Selective Oxidation of Olefins with Hydrogen Peroxide. *J. Catal.* **2005**, *229*, 490−498.

(9) Ziolek, M.; Decyk, P.; Sobczak, I.; Trejda, M.; Florek, J.; Golinska, H.; Klimas, H.; Wojtaszek, A. Catalytic Performance of Niobium Species in Crystalline and Amorphous Solids—Gas and Liquid Phase Oxidation. *Appl. Catal. A-Gen* **2011**, *391*, 194−204.

(10) Thornburg, N. E.; Nauert, S. L.; Thompson, A. B.; Notestein, J. M. Synthesis-Structure−Function Relationships of Silica-Supported Niobium(V) Catalysts for Alkene Epoxidation with H_2O_2. *ACS Catal.* **2016**, *6*, 6124−6134.

(11) Copéret, C.; Comas-Vives, A.; Conley, M. P.; Estes, D. P.; Fedorov, A.; Mougel, V.; Nagae, H.; Núñez-Zarur, F.; Zhizhko, P. A. Surface Organometallic and Coordination Chemistry toward Single-Site Heterogeneous Catalysts: Strategies, Methods, Structures, and Activities. *Chem. Rev.* **2016**, *116*, 323−421.

(12) Zhuravlev, L. The Surface Chemistry of Amorphous Silica. Zhuravlev Model. *Colloids Surf., A* **2000**, *173*, 1−38.

(13) Humbert, B. Estimation of Hydroxyl Density at the Surface of Pyrogenic Silicas by Complementary NMR and Raman Experiments. *J. Non-Cryst.* **1995**, *191*, 29−37.

(14) Lee, E. L.; Wachs, I. E. In Situ Spectroscopic Investigation of the Molecular and Electronic Structures of SiO_2 Supported Surface Metal Oxides. *J. Phys. Chem. C* **2007**, *111*, 14410−14425.

(15) Burneau, A.; Lalevée, J.; Carteret, C. Infrared Spectroscopic Study of the Formation of Reactive Silica by Pyrolysis in Vacuo of a Trimethylsiloxylated Sample. *J. Phys. Chem. B* **2000**, *104*, 990−996.

(16) Chen, C.; Mentink-Vigier, F.; Trébosc, J.; Goldberga, I.; Gaveau, P.; Thomassot, E.; Iuga, D.; Smith, M. E.; Chen, K.; Gan, Z.; et al. Labeling and Probing the Silica Surface Using Mechanochemistry and ^{17}O NMR Spectroscopy. *Chem.—Eur. J.* **2021**, *27*, 12574−12588.

(17) Boccuzzi, F.; Coluccia, S.; Ghiotti, G.; Morterra, C.; Zecchina, A. Infrared Study of Surface Modes on Silica. *J. Phys. Chem.* **1978**, *82*, 1298−1303.

(18) Morrow, B. A.; Cody, I. A. Infrared Study of Some Reactions with Reactive Sites on Dehydroxylated Silica. *J. Phys. Chem.* **1975**, *79*, 761−762.

(19) Inaki, Y.; Yoshida, H.; Yoshida, T.; Hattori, T. Active Sites on Mesoporous and Amorphous Silica Materials and Their Photocatalytic Activity: An Investigation by FTIR, ESR, VUV-UV and Photoluminescence Spectroscopies. *J. Phys. Chem. B* **2002**, *106*, 9098−9106.

(20) Zecchina, A.; Groppo, E.; Damin, A.; Prestipino, C. *Surface and Interfacial Organometallic Chemistry and Catalysis*; Copéret, C., Chaudret, B., Eds.; Springer-Verlag: Berlin/Heidelberg, 2005; Vol. *16*, pp 1−35.

(21) Garofalini, S. H. A Molecular Dynamics Simulation of the Vitreous Silica Surface. *J. Chem. Phys.* **1983**, *78*, 2069−2072.

(22) Levine, S. M.; Garofalini, S. H. A Structural Analysis of the Vitreous Silica Surface via a Molecular Dynamics Computer Simulation. *J. Chem. Phys.* **1987**, *86*, 2997−3002.

(23) Chenoweth, K.; van Duin, A. C. T.; Goddard, W. A. ReaxFF Reactive Force Field for Molecular Dynamics Simulations of Hydrocarbon Oxidation. *J. Phys. Chem. A* **2008**, *112*, 1040−1053.

(24) Fogarty, J. C.; Aktulga, H. M.; Grama, A. Y.; van Duin, A. C. T.; Pandit, S. A. A Reactive Molecular Dynamics Simulation of the Silica-Water Interface. *J. Chem. Phys.* **2010**, *132*, 174704.

(25) Gonçalves, W.; Morthomas, J.; Chantrenne, P.; Perez, M.; Foray, G.; Martin, C. L. Molecular Dynamics Simulations of Amorphous Silica Surface Properties with Truncated Coulomb Interactions. *J. Non-Cryst. Sol.* **2016**, *447*, 1−8.
(26) Rimsza, J. M.; Yeon, J.; van Duin, A. C. T.; Du, J. Water Interactions with Nanoporous Silica: Comparison of ReaxFF and *Ab Initio* Based Molecular Dynamics Simulations. *J. Phys. Chem. C* **2016**, *120*, 24803−24816.
(27) Yeon, J.; van Duin, A. C. T. ReaxFF Molecular Dynamics Simulations of Hydroxylation Kinetics for Amorphous and Nano-Silica Structure, and Its Relations with Atomic Strain Energy. *J.Phys. Chem. C* **2016**, *120*, 305−317.
(28) Mahadevan, T. S.; Du, J. Evaluating Water Reactivity at Silica Surfaces Using Reactive Potentials. *J. Phys. Chem. C* **2018**, *122*, 9875−9885.
(29) Wimalasiri, P. N.; Nguyen, N. P.; Senanayake, H. S.; Laird, B. B.; Thompson, W. H. Amorphous Silica Slab Models with Variable Surface Roughness and Silanol Density for Use in Simulations of Dynamics and Catalysis. *J. Phys. Chem. C* **2021**, *125*, 23418−23434.
(30) Caricato, M. Cluster Model Simulations of Metal-Doped Amorphous Silicates for Heterogeneous Catalysis. *J. Phys. Chem. C* **2021**, *125*, 27509−27519.
(31) Jystad, A. M.; Biancardi, A.; Caricato, M. Simulations of Ammonia Adsorption for the Characterization of Acid Sites in Metal-Doped Amorphous Silicates. *J. Phys. Chem. C* **2017**, *121*, 22258−22267.
(32) Jystad, A.; Leblanc, H.; Caricato, M. Surface Acidity Characterization of Metal-Doped Amorphous Silicates via Py-FTIR and ^{15}N NMR Simulations. *J. Phys. Chem. C* **2020**, *124*, 15231−15240.
(33) Khan, S. A.; Vandervelden, C. A.; Scott, S. L.; Peters, B. Grafting Metal Complexes onto Amorphous Supports: From Elementary Steps to Catalyst Site Populations via Kernel Regression. *React. Chem. Eng.* **2020**, *5*, 66−76.
(34) Vandervelden, C. A.; Khan, S. A.; Scott, S. L.; Peters, B. Site-Averaged Kinetics for Catalysts on Amorphous Supports: An Importance Learning Algorithm. *React. Chem. Eng.* **2020**, *5*, 77−86.
(35) Vandervelden, C.; Jystad, A.; Peters, B.; Caricato, M. Predicted Properties of Active Catalyst Sites on Amorphous Silica: Impact of Silica Preoptimization Protocol. *Ind. Eng. Chem. Res.* **2021**, *60*, 12834−12846.
(36) Tielens, F.; Gierada, M.; Handzlik, J.; Calatayud, M. Characterization of Amorphous Silica Based Catalysts Using DFT Computational Methods. *Catal. Today* **2020**, *354*, 3−18.
(37) van Beest, B. W. H.; Kramer, G. J.; van Santen, R. A. Force Fields for Silicas and Aluminophosphates Based on *Ab Initio* Calculations. *Phys. Rev. Lett.* **1990**, *64*, 1955−1958.
(38) van Duin, A. C. T.; Dasgupta, S.; Lorant, F.; Goddard, W. A. ReaxFF: A Reactive Force Field for Hydrocarbons. *J. Phys. Chem. A* **2001**, *105*, 9396−9409.
(39) van Duin, A. C. T.; Strachan, A.; Stewman, S.; Zhang, Q.; Xu, X.; Goddard, W. A. ReaxFF$_{SiO}$ Reactive Force Field for Silicon and Silicon Oxide Systems. *J.Phys. Chem. A* **2003**, *107*, 3803−3811.
(40) Lee, S. H.; Stewart, R. J.; Park, H.; Goyal, S.; Botu, V.; Kim, H.; Min, K.; Cho, E.; Rammohan, A. R.; Mauro, J. C. Effect of Nanoscale Roughness on Adhesion between Glassy Silica and Polyimides: A Molecular Dynamics Study. *J. Phys. Chem. C* **2017**, *121*, 24648−24656.
(41) Karma, A. Fluctuations in Solidification. *Phys. Rev. E* **1993**, *48*, 3441−3458.
(42) Hoyt, J. J.; Asta, M.; Karma, A. Method for Computing the Anisotropy of the Solid-Liquid Interfacial Free Energy. *Phys. Rev. Lett.* **2001**, *86*, 5530−5533.
(43) Freitas, R.; Frolov, T.; Asta, M. Capillary Fluctuations of Surface Steps: An Atomistic Simulation Study for the Model Cu(111) System. *Phys. Rev. E* **2017**, *96*, 043308.
(44) Amini, M.; Laird, B. B. Kinetic Coefficient for Hard-Sphere Crystal Growth from the Melt. *Phys. Rev. Lett.* **2006**, *97*, 216102.
(45) Rimsza, J.; Du, J. *Ab Initio* Molecular Dynamics Simulations of the Hydroxylation of Nanoporous Silica. *J. Am. Ceram. Soc.* **2015**, *98*, 3748−3757.
(46) Rimsza, J. M.; Jones, R. E.; Criscenti, L. J. Surface Structure and Stability of Partially Hydroxylated Silica Surfaces. *Langmuir* **2017**, *33*, 3882−3891.
(47) Yeon, J.; van Duin, A. C. T.; Kim, S. H. Effects of Water on Tribochemical Wear of Silicon Oxide Interface: Molecular Dynamics (MD) Study with Reactive Force Field (ReaxFF). *Langmuir* **2016**, *32*, 1018−1026.
(48) Thompson, A. P.; Aktulga, H. M.; Berger, R.; Bolintineanu, D. S.; Brown, W. M.; Crozier, P. S.; in 't Veld, P. J.; Kohlmeyer, A.; Moore, S. G.; Nguyen, T. D.; et al. LAMMPS—a Flexible Simulation Tool for Particle-Based Materials Modeling at the Atomic, Meso, and Continuum Scales. *Comput. Phys. Commun.* **2022**, *271*, 108171.
(49) Rozas, R.; Horbach, J. Capillary wave analysis of rough solid-liquid interfaces in nickel. *Europhys. Lett.* **2011**, *93*, 26006.
(50) Martínez, L.; Andrade, R.; Birgin, E. G.; Martínez, J. M. PACKMOL: A Package for Building Initial Configurations for Molecular Dynamics Simulations. *J. Comput. Chem.* **2009**, *30*, 2157−2164.
(51) Mozzi, R. L.; Warren, B. E. The Structure of Vitreous Silica. *J. Appl. Crystallogr.* **1969**, *2*, 164−172.
(52) Henke, L.; Nagy, N.; Krull, U. J. An AFM Determination of the Effects on Surface Roughness Caused by Cleaning of Fused Silica and Glass Substrates in the Process of Optical Biosensor Preparation. *Biosens. Bioelectron.* **2002**, *17*, 547−555.
(53) Chacón, E.; Tarazona, P. Characterization of the Intrinsic Density Profiles for Liquid Surfaces. *J. Phys.: Condens. Matter* **2005**, *17*, S3493−S3498.
(54) Du, J.; Cormack, A. N. Molecular Dynamics Simulation of the Structure and Hydroxylation of Silica Glass Surfaces. *J. Am. Ceram. Soc.* **2005**, *88*, 2532−2539.
(55) Rino, J. P.; Ebbsjö, I.; Kalia, R. K.; Nakano, A.; Vashishta, P. Structure of Rings in Vitreous SiO 2. *Phys. Rev. B: Condens. Matter Mater. Phys.* **1993**, *47*, 3053−3062.
(56) Feuston, B. P.; Garofalini, S. H. Topological and Bonding Defects in Vitreous Silica Surfaces. *J. Chem. Phys.* **1989**, *91*, 564−570.
(57) Roder, A.; Kob, W.; Binder, K. Structure and Dynamics of Amorphous Silica Surfaces. *J. Chem. Phys.* **2001**, *114*, 7602−7614.
(58) D'Souza, A. S.; Pantano, C. G. Mechanisms for Silanol Formation on Amorphous Silica Fracture Surfaces. *J. Am. Ceram. Soc.* **1999**, *82*, 1289−1293.
(59) Machacek, J.; Gedeon, O.; Liska, M. Molecular Approach to the 5-Coordinated Silicon Atoms in Silicate Glasses. *Phys. Chem. Glasses-B* **2007**, *48*, 345−353.
(60) Yuan, X.; Cormack, A. Local Structures of MD-modeled Vitreous Silica and Sodium Silicate Glasses. *J. Non-Cryst.* **2001**, *283*, 69−87.
(61) Stebbins, J. F.; McMillan, P. Compositional and Temperature Effects on Five-Coordinated Silicon in Ambient Pressure Silicate Glasses. *J. Non-Cryst.* **1993**, *160*, 116−125.
(62) Swamy, K. C. K.; Chandrasekhar, V.; Harland, J. J.; Holmes, J. M.; Day, R. O.; Holmes, R. R. Pentacoordinated Molecules. 79. Pentacoordinate Acyclic and Cyclic Anionic Oxysilicates. A Silicon-29 NMR and x-Ray Structural Study. *J. Am. Chem. Soc.* **1990**, *112*, 2341−2348.
(63) Siodla, T.; Sobczak, I.; Ziolek, M.; Tielens, F. Theoretical and Experimental Insight into Zinc Loading on Mesoporous Silica. *Microporous Mesoporous Mater.* **2018**, *256*, 199−205.
(64) Galeener, F. L. Planar Rings in Vitreous Silica. *J. Non-Cryst.* **1982**, *49*, 53−62.
(65) Brinker, C.; Brow, R.; Tallant, D.; Kirkpatrick, R. Surface structure and chemistry of high surface area silica gels. *J. Non-Cryst.* **1990**, *120*, 26−33.
(66) DeMayo, P.; Natarajan, L.; Ware, W. R. Surface Photochemistry: Temperature Effects on the Emission of Aromatic Hydrocarbons Adsorbed on Silica Gel. *ACS Symp. Ser.* **1985**, *278*, 1−19.

https://doi.org/10.1021/acs.jpca.3c04955
J. Phys. Chem. A 2023, 127, 9831−9841

(67) Grillo, M. E.; Coll, D. S.; Rodríguez, J. Effect of the environment on the hydroxyl density of α-quartz (111). *Chem. Phys. Lett.* **2012**, *522*, 46−50.
(68) Murashov, V. V.; Demchuk, E. Surface Sites and Unrelaxed Surface Energies of Tetrahedral Silica Polymorphs and Silicate. *Surf. Sci.* **2005**, *595*, 6−19.
(69) De Leeuw, N. H.; Higgins, F. M.; Parker, S. C. Modeling the Surface Structure and Stability of α-Quartz. *J. Phys. Chem. B* **1999**, *103*, 1270−1277.
(70) Murashov, V. V. Reconstruction of Pristine and Hydrolyzed Quartz Surfaces. *J. Phys. Chem. B* **2005**, *109*, 4144−4151.
(71) Zhuravlev, L. T. Concentration of Hydroxyl Groups on the Surface of Amorphous Silicas. *Langmuir* **1987**, *3*, 316−318.
(72) Shchipalov, Y. K. Surface Energy of Crystalline and Vitreous Silica. *Glass Ceram+* **2000**, *57*, 374−377.
(73) Bergna, H. E. *The Colloid Chemistry of Silica*; American Chemical Society, 1989; pp 1−47, Chapter 1.
(74) Bunker, B. C.; Haaland, D. M.; Michalske, T. A.; Smith, W. L. Kinetics of dissociative chemisorption on strained edge-shared surface defects on dehydroxylated silica. *Surf. Sci.* **1989**, *222*, 95−118.
(75) D'Souza, A. S.; Pantano, C. G. Hydroxylation and Dehydroxylation Behavior of Silica Glass Fracture Surfaces. *J. Am. Ceram. Soc.* **2002**, *85*, 1499−1504.
(76) D'Souza, A. S.; Pantano, C. G.; Kallury, K. M. R. Determination of the Surface Silanol Concentration of Amorphous Silica Surfaces Using Static Secondary Ion Mass Spectroscopy. *J. Vac. Sci. Technol.* **1997**, *15*, 526−531.
(77) Pfeiffer-Laplaud, M.; Costa, D.; Tielens, F.; Gaigeot, M.-P.; Sulpizi, M. Bimodal Acidity at the Amorphous Silica/Water Interface. *J. Phys. Chem. C* **2015**, *119*, 27354−27362.
(78) Sulpizi, M.; Gaigeot, M.-P.; Sprik, M. The Silica−Water Interface: How the Silanols Determine the Surface Acidity and Modulate the Water Properties. *J. Chem. Theory Comput.* **2012**, *8*, 1037−1047.
(79) Ostroverkhov, V.; Waychunas, G. A.; Shen, Y. R. New Information on Water Interfacial Structure Revealed by Phase-Sensitive Surface Spectroscopy. *Phys. Rev. Lett.* **2005**, *94*, 046102.
(80) Gierada, M.; De Proft, F.; Sulpizi, M.; Tielens, F. Understanding the Acidic Properties of the Amorphous Hydroxylated Silica Surface. *J. Phys. Chem. C* **2019**, *123*, 17343−17352.

https://doi.org/10.1021/acs.jpca.3c04955
J. Phys. Chem. A 2023, 127, 9831−9841